

Möbius transformation and coupled-wave theory: Complete identification of the transfer matrixStefanos Fr. Koufidis * and Martin W. McCall *Blackett Laboratory, Department of Physics, Imperial College of Science, Technology and Medicine,
Prince Consort Road, London SW7 2AZ, United Kingdom* (Received 20 October 2022; accepted 28 November 2022; published 19 December 2022)

A Möbius transformation which conformally maps the unit circle onto itself is applied to the scalar coupled-wave equations, describing electromagnetic wave propagation in Bragg gratings, and reduces them to a first-order nonlinear differential equation of a single real variable. This equation is analytically integrated for linear detuning and numerically for more complicated refractive index modulation scenarios, e.g., chirped and apodized Bragg gratings, offering a platform for identifying both the amplitude and phase of all elements of the transfer matrix of arbitrarily complex cases. A link between coupled-wave theory and coupled oscillators is established, and exploring the transformation's geometrical properties leads to alternative definitions of the photonic band gap.

DOI: [10.1103/PhysRevA.106.062213](https://doi.org/10.1103/PhysRevA.106.062213)**I. INTRODUCTION**

Uniform Bragg gratings are transparent photonic devices with a periodic modulation of their refractive index where for incident monochromatic light, successive reflections add up coherently to give a strong reflection around the Bragg wavelength $\lambda_0 = 2\bar{n}\Lambda$, where \bar{n} is the average refractive index and Λ is the grating spatial period [1]. They can be written via the diffraction pattern from a phase mask illuminated by UV light [2] and their wavelength-dependent nature resembles Fabry-Pérot étalons, providing less-alignment-sensitive spatial filters in the visible spectrum which can be easily incorporated in photonic structures. Chirped Bragg gratings are used as resonators to produce a wide variety of free spectral ranges in [3] and various narrowband channels of roughly equal spacing in fiber lasers in [4]. They can be tailored to reduce undesirable spectral side lobes [5], stabilize the single-mode output of continuous-wave fiber lasers [6], and control dispersion. Indeed, in [7] linearly chirped Bragg gratings cancel the dispersion of optical waveguides, while in [8] they determine the pulse width and energy in fiber soliton lasers. Phase-shifted gratings minimize channel spacing of wavelength division multiplexers in [9] and they are used as all-fiber demultiplexers of optical systems with multiple channels in [10]. The effect of the number of phase shifts on the transmission spectrum of Bragg filters is explored in [11].

Coupled-wave theory (CWT) is the principal approximation for obtaining the optical spectrum of Bragg gratings. The coupled-wave equations (CWEs) match synchronous terms derived from the Helmholtz wave equation, assuming weak amplitude of the refractive index modulation and under the slowly varying envelope approximation [12]. They can be analytically integrated in special cases (e.g., weak or uniform gratings) and numerically in the rest. Some modified, semianalytical, and CWT-based approaches for high-contrast

refractive index modulation are discussed in [13]. An example considering higher-order phenomena and effective-medium theory to analyze nonuniform gratings is found in [14]. In [5] a transformation reduces the CWEs to a Riccati equation and in [15] the propagation in nonlinear Bragg gratings is exactly solved via the so-called method of single expression for the electric field which does not consider counterpropagating modes. A classic approach is seen in [16,17] where a nonuniform grating slab waveguide is divided into N cascaded quasiuniform divisions. Thereafter, the compound structure's optical response is approximated by multiplying all uniform segments transfer matrices \mathbf{S}_i , known from CWT, to form the overall transfer matrix \mathbf{S} . This is in principle a reliable and fast method, albeit troublesome in cases of long gratings with many periods [12]. The transfer-matrix method is closely correlated to CWT but contains some ambiguities which are clarified in [18].

For dynamical systems described by N coupled equations of N -dimensional parameters, reducing the order leads to significant simplifications. In [19] a nonlinear coordinate transformation reduces a system of ($N \geq 3$)-dimensional coupled oscillators (Kuramoto model) to $N = 3$ dimensions, proved in [20] to be integrable Riccati equations. This method resembles that of [21,22] where group theory is utilized to identify underlying symmetries in four-wave mixing, also parametrizing the problem using only three variables. In [23] exploring the action of a subgroup of Möbius transformations, which conformally map the unit disk onto itself, offers insights into the reduction mechanism: It is related to the mapping on the Möbius group being a three-dimensional Lie group.

Inspired by the above, we explore the action of a Möbius transformation that preserves the unit circle to the CWEs. The paper is organized as follows: In Sec. II we discuss challenges in solving CWEs and in Sec. III scrutinizing the underlying symmetries of the system leads to a particular Möbius transformation that reduces the CWEs to a first-order nonlinear differential equation of a single real variable which

*steven.koufidis20@imperial.ac.uk

encodes all spectral information. Geometrical properties of the transformation lead to identification of both the amplitude and phase of all elements of the transfer matrix for arbitrarily complex refractive index modulation scenarios. This equation is analytically integrated for uniform Bragg gratings in Sec. IV where it is also related to the Adler equation of classic oscillators theory. Insights regarding the photonic band gap are revealed and alternative definitions of the Bragg zone are given. The nonlinear equation is numerically integrated in Sec. V where the method's success is demonstrated in chirped, apodized, and cascaded Bragg gratings of slightly dissimilar pitches. We summarize in Sec. VI.

II. CHALLENGES IN SOLVING COUPLED-WAVE EQUATIONS

The CWEs describing the propagation of the forward and backward electric field amplitudes A^\pm in a scalar Bragg grating can be expressed in a vectorial-differential notation as

$$\frac{d\mathbf{A}}{dz} = \mathbf{M} \cdot \mathbf{A}, \quad (1)$$

where $\mathbf{A} = (A^+ A^-)^\top$, with \top denoting transpose, and the characteristic matrix of the system is

$$\mathbf{M} = \begin{pmatrix} 0 & i\kappa e^{-i\varphi} \\ -i\kappa e^{i\varphi} & 0 \end{pmatrix}.$$

Here $\kappa \approx \pi \delta \bar{n} / \lambda_0$ is the grating coupling coefficient, with $\delta \bar{n}$ the amplitude of the refractive index modulation. Unless we are interested in apodized gratings, κ will be assumed constant and generally complex in the presence of loss or gain. If z_0 is the grating initial point, the z -dependent phase term $\varphi \equiv \varphi(z)$ accounts for the refractive index variation along the grating length and is defined as [7]

$$\varphi(z) = \int_{z_0}^z B(s) ds, \quad (2)$$

where $B(z) = 2\bar{n}k_0 - K(z)$, with k_0 the free-space wave number. The grating local spatial frequency is $K(z) = K_0 + \Delta K(z)$, where $K_0 = 2\pi/\Lambda$ is constant and $\Delta K(z)$ can be seen as a perturbation [5].

Let \mathbf{A}_0 express some known initial conditions at z_0 . Then the solution to Eq. (1) may take the matrix-exponential form

$$\mathbf{A}(z) = \exp\left(\int_{z_0}^z \mathbf{M}(s) ds\right) \mathbf{A}_0, \quad (3)$$

only in the on-resonance case, where $\varphi = 0$, and the system of Eq. (1) has constant coefficients. This is not true, however, when the phase term is a nonzero function of the grating length $\varphi(z)$ since the characteristic matrix \mathbf{M} does not generally commute with its integral at every point of its definition domain, i.e.,

$$\mathbf{M}(z) \left(\int_{z_0}^z \mathbf{M}(s) ds \right) \neq \left(\int_{z_0}^z \mathbf{M}(s) ds \right) \mathbf{M}(z), \quad (4)$$

where the integration is performed element-by-element.

In uniform gratings, $\Delta K = 0$ and the inequality (4) is an equality only at the discrete points $\varphi = 2\nu\pi$, $\nu \in \mathbb{N}$, or trivially when $\kappa = 0$. Nonetheless, the exponential approximation can be within an acceptable error margin for small values of

both the grating length L (typically a few millimeters) and $\delta \bar{n}$, giving a slightly smaller optical bandwidth compared to that accessed via classic CWT solution methods. With an increment of L or $\delta \bar{n}$, within the usual approximation limits of CWT, the discrepancy of the two bandwidths scales with L and κ^2 , respectively, and the mismatch of relation (4) increases. Hence, although the use of the simple equation (3) for numerical integration is tempting, the noncommutative property should not be disregarded unless the grating is uniform, small, and weak.

The integration approach of Eq. (3) for analyzing nonuniform fiber Bragg gratings appears to have been first proposed in [24] and subsequently used in [25] to solve the CWEs for gratings with an acoustically induced microbending. In both cases, the noncommutative property expressed via the inequality (4) was neglected, leading to minor inconsistencies between the theoretically predicted and the experimentally realized optical spectra. Eventually, the authors improved their method in [26] by dividing the total integration length into multiple parts so that \mathbf{M} approximately commutes with its integral at each sublength.

Whether the grating characteristics render the approximation of Eq. (3) acceptable or not, or someone resorts to the brute force of direct numerical integration of Eq. (1), guessing the initial conditions is essential [27] but nontrivial, especially when physical arguments must be considered. Such methods are usually slow [12] as they require integration of a system of differential equations which are in principle both nonlinear and complex. Additionally, they are in need of an adaptive step size, which may affect the stability of the algorithm [28]. It will soon become apparent that the system of Eq. (1) can be naturally reduced to one nonlinear differential equation of a single real variable whereby once it is integrated, both the amplitude and phase of all elements of the solution matrix can be algebraically determined via simple formulas.

Although we will be mostly concerned with the CWEs description of Eq. (1), it is worth mentioning the widely adopted method for solving CWEs, seen, e.g., in [9,10,12], which uses the auxiliary fields $\tilde{A}^+ = \exp(i\varphi/2)A^+$ and $\tilde{A}^- = \exp(-i\varphi/2)A^-$ to transform the system of Eq. (1) to the equivalent

$$\frac{d}{dz} \begin{pmatrix} \tilde{A}^+ \\ \tilde{A}^- \end{pmatrix} = \begin{pmatrix} \frac{i}{2} \frac{d\varphi}{dz} & i\kappa \\ -i\kappa & -\frac{i}{2} \frac{d\varphi}{dz} \end{pmatrix} \begin{pmatrix} \tilde{A}^+ \\ \tilde{A}^- \end{pmatrix}. \quad (5)$$

Then, in uniform gratings, the system of Eq. (5) has constant coefficients and the matrix-exponential form of Eq. (3) is a well-defined analytic function of the transformed system's characteristic matrix $\tilde{\mathbf{M}}$. For φ a slowly varying function of z , defining the local reflection coefficient $r = \tilde{A}^- / \tilde{A}^+$, as in [5,29], reduces the system of Eq. (5) to a complex Riccati equation, and this reduction mechanism will be naturally associated with the system's underlying symmetries in this paper.

With an analytic solution for uniform gratings known, we can employ the so-called piecewise transfer-matrix approach to examine nonuniform cases. Indeed, partitioning the total length L in such way that each sublength $l_i < \pi/2L$ forms a quasiuniform segment of approximately constant period, we can obtain the overall transfer matrix by cascading all transfer matrices of the roughly uniform divisions. Although this is an effective method, it is problematic in gratings with

many periods (greater than 10^5 [12]). Additionally, it contains some pitfalls which lead to overlooking important physical phenomena, evident in cascaded gratings with slightly dissimilar pitches or in gratings delineated by a phase discontinuity, as discussed in Sec. VC. Our method does not impose such restrictions; being not inherently discrete (N.B. a certain discretization is of course required for numerical integration), it can indeed lift any length limitations as the number of periods is irrelevant. Moreover, it hides any complexity of the cascaded matrices strict mathematical formalism.

III. MÖBIUS TRANSFORMATION METHOD

A. Transfer-matrix symmetries

Setting the grating initial point at $z_0 = 0$, the overall solution to Eq. (1) can be explicitly written as

$$\mathbf{A}(z) = \mathbf{S}(z)\mathbf{A}_0, \quad \forall z \in [0, +\infty), \quad (6)$$

where evidently the propagator \mathbf{S} is a transfer matrix relating the amplitudes of the electric fields at the output of the grating ($z = L$) to those at the input ($z_0 = 0$). It then follows from Eq. (1) that \mathbf{S} solves

$$\frac{d\mathbf{S}}{dz} = \mathbf{M} \cdot \mathbf{S}. \quad (7)$$

According to Liouville's formula [see Eq. (1.5) in [27]],

$$\det[\mathbf{S}(z)] = \det[\mathbf{S}(0)] \exp\left(\int_0^z \text{tr}[\mathbf{M}(s)]ds\right), \quad (8)$$

and for \mathbf{M} traceless, the determinant of the fundamental matrix (Wronskian) is always constant, no matter if loss or gain is considered. It is then implied by Eq. (6) that $\mathbf{S}(0) = \mathbb{I}$, where \mathbb{I} is the 2×2 identity, leading via Eq. (8) to the first symmetry relation

$$\det(\mathbf{S}) = 1. \quad (9)$$

In fact, unimodularity is a fundamental property of traceless characteristic matrices and will also hold in cases of loss and gain modulated gratings [cf. Eqs. (6) and (7) in [30]]. Nevertheless, it cannot guarantee reciprocity on its own.

Furthermore, for \bar{n} , $\delta\bar{n} \in \mathbb{R}$, meaning also that $\varphi, \kappa \in \mathbb{R}$, the matrix \mathbf{M} is Hermitian, or $\mathbf{M} = \mathbf{M}^\dagger$, where the dagger is the Hermitian adjoint. It is then easy to prove that $\mathbf{A}^\dagger \cdot \mathbf{J} \cdot \mathbf{A}$, where $\mathbf{J} = \begin{pmatrix} 1 & 0 \\ 0 & -1 \end{pmatrix}$, is conserved, slightly different from [22] and for two modes interfering. Indeed, for \mathbf{M} Hermitian and the adjoint acting on each component of $(dA^+/dz \ dA^-/dz)^\top$, we have

$$\frac{d}{dz}(\mathbf{A}^\dagger \cdot \mathbf{J} \cdot \mathbf{A}) = \mathbf{A}^\dagger \cdot (\mathbf{M} \cdot \mathbf{J} + \mathbf{J} \cdot \mathbf{M}) \cdot \mathbf{A}. \quad (10)$$

Since \mathbf{M} is also anti-diagonal, the matrix $\mathbf{M} \cdot \mathbf{J}$ is skew Hermitian, or $(\mathbf{M} \cdot \mathbf{J})^\dagger = -\mathbf{M} \cdot \mathbf{J}$, and Eq. (10) yields

$$\frac{d}{dz}(\mathbf{A}^\dagger \cdot \mathbf{J} \cdot \mathbf{A}) = \mathbf{0}.$$

Hence, $\mathbf{A}^\dagger \cdot \mathbf{J} \cdot \mathbf{A}$ is conserved and $I_0 = |A^+|^2 - |A^-|^2$ is constant, in agreement with Eq. (9) in [31] for counterpropagating modes. This expresses energy (flux) conservation. If $\mathbf{A}^\dagger \cdot \mathbf{J} \cdot \mathbf{A}$ is conserved, so is $\mathbf{S}^\dagger \cdot \mathbf{J} \cdot \mathbf{S}$ and for $\mathbf{S}(0) = \mathbb{I}$ we end up with

the second symmetry relation

$$\mathbf{S}^\dagger \cdot \mathbf{J} \cdot \mathbf{S} = \mathbf{J}. \quad (11)$$

The conditions of Eqs. (9) and (11) are sufficient to guarantee that $\mathbf{S} \in \text{SU}(1, 1)$, where $\text{SU}(1, 1)$ is the special unitary group defined in [32] as the set of all 2×2 matrices \mathbf{U} with unit determinant such that $\mathbf{U}^\dagger \cdot \mathbf{J} \cdot \mathbf{U} = \mathbf{J}$. These are symmetry-based arguments that lead to the same conclusions reached in [33] where the form of \mathbf{S} is attributed to energy conservation and time-reversal invariance, which is equivalent to reciprocity *only* in energy-conserving systems [34]. Details on transfer-matrix group-theory symmetries can be found in Appendix A in [35] and a comprehensive discussion of their geometrical aspects in [36].

B. Reducing the coupled-wave equations

It is straightforward to show from Eqs. (9) and (11) that the representation of the $\text{SU}(1, 1)$ group takes the well-known form

$$\mathbf{S} = \begin{pmatrix} P & Q \\ Q^* & P^* \end{pmatrix}, \quad |P|^2 - |Q|^2 = 1, \quad (12)$$

where the asterisk denotes complex conjugation. By converting the transfer matrix \mathbf{S} to a scattering matrix \mathbf{S}_s via Eqs. (69)–(72) in [34], we can verify that both the energy-conservation condition $\mathbf{S}_s \mathbf{S}_s^\dagger = \mathbb{I}$ (unitary) and the reciprocity condition $\mathbf{S}_s = \mathbf{S}_s^\top$ (orthogonal) are satisfied.

The matrix representation of Eq. (12) can be naturally associated with a Möbius transformation $w = w(w_0) : \text{SU}(1, 1) \rightarrow \mathbb{C}$, as in [37], defined via

$$w(w_0) = \frac{Pw_0 + Q}{Q^*w_0 + P^*}, \quad |P|^2 - |Q|^2 = 1; \quad w, w_0 \in \mathbb{C}, \quad (13)$$

which maps the unit disk $\mathcal{D} = \{|w_0| < 1, w_0 \in \mathbb{C}\}$ and its boundary $\partial\mathcal{D} = \{|w_0| = 1, w_0 \in \mathbb{C}\}$ conformally onto themselves [38]. In fact, the pseudounitary group $\text{SU}(1, 1)$ is isomorphic to $\text{SL}(2, \mathbb{R})$, the set of all real-valued matrices with unit determinant [32], and represents the most general isometric distortion of the upper half plane. As shown in Chap. 1, Pt. 4 in [32], this isomorphism is achieved via

$$\begin{pmatrix} P & Q \\ Q^* & P^* \end{pmatrix} = \frac{1}{\sqrt{2}} \begin{pmatrix} 1 & -i \\ -i & 1 \end{pmatrix} \begin{pmatrix} \alpha & \beta \\ \gamma & \delta \end{pmatrix} \frac{1}{\sqrt{2}} \begin{pmatrix} 1 & i \\ i & 1 \end{pmatrix},$$

where $\alpha\delta - \beta\gamma = 1$ with $\alpha, \beta, \gamma, \delta \in \mathbb{R}$. The $\text{SU}(2)$ matrices pre- and postmultiplying the real-valued matrix are isomorphic to rotations by $\pi/2$ in $\text{SO}(3)$. Under a stereographic projection, these will first take the unit disk into the upper half plane to be distorted before returning the distorted upper half plane to the unit disk, hence preserving it. For its boundary $\partial\mathcal{D}$, it is easy to verify that $|w[\exp(i\theta)]| = 1$, $\theta \in \mathbb{R}$.

Combining now Eqs. (7) and (12) yields

$$\frac{dP}{dz} = i\kappa e^{-i\varphi} Q^* \quad \text{and} \quad \frac{dQ}{dz} = i\kappa e^{-i\varphi} P^*.$$

Then, the transformation of Eq. (13) determines that the newly introduced variable w evolves according to the complex

Riccati equation

$$\frac{dw}{dz} = i\kappa(e^{-i\varphi} + e^{i\varphi}w^2), \quad (14)$$

which appears like Eq. (12) in [5] but with opposite signs in the exponential terms. However, here w and w_0 have the physical meaning of the local (at some point z) and initial (precisely at $z_0 = 0$) conductance $\rho = A^+/A^-$, respectively, and *not* reflectance. As Eq. (14) was deduced via the Möbius transformation of Eq. (13), this clearly establishes a geometrical approach in examining the spectral characteristics of Bragg gratings, similar to the usual admittance Y Smith chart used in electrical engineering to examine transmission lines [39]. Crucially, (A^+, A^-) are the homogeneous coordinates of w corresponding to a singular stereographic projection, provided $(A^+, A^-) \neq (0, 0)$ [40]. We underline that Eq. (14) will still hold if the coupling coefficient is z -dependent.

Should we confine the action of Eq. (13) to the invariant under the transformation unit circle $\partial\mathcal{D}$ ($|w_0| = 1$), the symmetries of the system imply that $|w| = 1$. This of course restricts the space of the solutions to those of energy-conserving systems. It is then convenient to set $w = \exp(i\psi)$, $\psi \in \mathbb{R}$, so that Eq. (14) simplifies to a first-order nonlinear differential equation of a single real variable which encodes all the information of the transfer matrix, namely,

$$\frac{d\psi}{dz} = 2\kappa \cos(\psi + \varphi), \quad \psi \in \mathbb{R}. \quad (15)$$

Remarkably, Eqs. (14) and (15) resemble Eqs. (23a) and (23b) in [23] or the equivalent, previously derived, Eqs. (10) and (11) in [41], respectively, which model coupled oscillators systems. In fact, our Eq. (15) is a special case of the aforementioned since it does not contain the extra term g of [23] and finding an analytic solution is plausible under corresponding preconditions (see Sec. IV). This is a consequence of the action of a Möbius transformation that preserves the open unit disk and its boundary. The reduction of the CWEs to a Riccati equation is consistent with the response of [20] to the coupled-oscillator problem in [19] and reveals the insights of the reduction mechanism via the local reflection coefficient of [5]. Additionally, in the framework of the linear classical spin Hamiltonian, Eq. (1) appears like the equation of motion [cf. Eq. (6) in [42]] with the solution taking the form of a Möbius transformation too.

C. Identifying the transfer matrix

The nonlinearity of Eq. (15) suggests that numerical techniques must be implemented. A recommendation could be MATLAB's ordinary differential equation (ODE) solvers which integrate $\psi' = \mathbf{F}(z, \psi)$ from z_0 to z_L , with an initial condition ψ_0 , via the Runge-Kutta iterative method. However, even if Eq. (15) is numerically solved, identifying both the amplitude and phase of the P and Q parameters, and thus the grating transfer matrix, is still a challenge. This can be overcome by exploring a fundamental property of linear fractional transformations.

In point of fact, the Möbius transformation

$$w_0 \rightarrow w : w = \frac{aw_0 + b}{cw_0 + d}, \quad ad \neq bc; a, b, c, d \in \mathbb{C}$$

is completely defined by the cross ratio

$$\frac{(w - w_1)(w_2 - w_3)}{(w - w_3)(w_2 - w_1)} = \frac{(w_0 - w_01)(w_02 - w_03)}{(w_0 - w_03)(w_02 - w_01)},$$

mapping finite distinct points w_{01} , w_{02} , and w_{03} of the w_0 plane onto finite distinct points w_1 , w_2 , and w_3 of the w plane [43]. Hence, a Möbius transformation is uniquely determined, up to an overall scaling, by its values at three pairs (w_{01}, w_1) , (w_{02}, w_2) , and (w_{03}, w_3) . Its coefficients are given by the determinants

$$a = \begin{vmatrix} w_{01}w_1 & w_1 & 1 \\ w_{02}w_2 & w_2 & 1 \\ w_{03}w_3 & w_3 & 1 \end{vmatrix}, \quad b = \begin{vmatrix} w_{01}w_1 & w_{01} & w_1 \\ w_{02}w_2 & w_{02} & w_2 \\ w_{03}w_3 & w_{03} & w_3 \end{vmatrix},$$

$$c = \begin{vmatrix} w_{01} & w_1 & 1 \\ w_{02} & w_2 & 1 \\ w_{03} & w_3 & 1 \end{vmatrix}, \quad \text{and} \quad d = \begin{vmatrix} w_{01}w_1 & w_{01} & 1 \\ w_{02}w_2 & w_{02} & 1 \\ w_{03}w_3 & w_{03} & 1 \end{vmatrix}. \quad (16)$$

To identify the elements of the transfer matrix, at least three images of three points are needed, as explained in Sec. 6 in [44] and Sec. 4 in [45], i.e., three pairs of (ψ_{0j}, ψ_j) , $j = 1, 2, 3$. Such identification is achieved by solving Eq. (15) three times, each with a different initial condition ψ_{0j} . This is appropriate since the physically meaningful boundary condition is that the local conductance at the end of the grating is infinite [impose $A^-(L) = 0$] and the ordered pair (A^+, A^-) no longer corresponds to a unique w , rendering ψ_0 indifferent. The values of ψ_{0j} lie in $(-\infty, +\infty)$ with $w_{0j} = \exp(i\psi_{0j})$ lying on the unit circle and can be arbitrarily chosen. We elect points of the upper half plane, say, $\psi_{01} = 0$, $\psi_{02} = \pi/2$, and $\psi_{03} = \pi$, but these can be any points as long as they are finite and discrete. Then the determinants of Eq. (16) provide us with a, b, c , and d .

Despite the Möbius transformation's uniqueness, its representation is only unique up to a complex multiplier [32]. Still, we can normalize its representation matrix to one with unit determinant and identify both the amplitude and phase of all elements of the transfer matrix as

$$\begin{pmatrix} P & Q \\ Q^* & P^* \end{pmatrix} = \frac{1}{(ad - bc)^{1/2}} \begin{pmatrix} a & b \\ c & d \end{pmatrix}.$$

Thereafter, the optical spectrum may be accessed via the reflection and transmission coefficients $r = -Q^*/P^*$ and $t = 1/P^*$, respectively.

Solving Eq. (15) three times seems less efficient than solving Eq. (14) once, as in [5]. In the latter, the intensity reflectance is directly retrieved as $R = rr^*$ whereas in energy-conserving systems, the intensity transmittance is simply $T = 1 - R$ and the optical spectrum is fully determined. Notwithstanding, the phase of the transmission coefficient, important in dispersion compensation, cannot be determined. Additionally, solving the Riccati equation (14) strongly depends on the initial condition guessing which in our method is unimportant. The most important aspect of our method lies in completely determining both the amplitude and phase of all elements of the transfer matrix which for this analysis is a three-dimensional Lie group, similarly to [23], with real parameters $|P|$, $\arg(P)$, and $\arg(Q)$. This proves beneficial in systems where the $SU(1, 1)$ symmetry is broken and the

reflection seen from the left, $r_L = -S_{21}/S_{22}$, may differ from the one seen from the right, $r_R = S_{12}/S_{22}$.

Such examples are Bragg gratings with modulated loss and gain [30], or as they later became known parity-time (\mathcal{PT}) symmetric Bragg gratings [46], which induce unidirectional invisibility despite satisfying Lorentz reciprocity [47]. In this instance, although the unimodularity condition of Eq. (9) will still hold, the Hermiticity condition of Eq. (11) breaks and $S \notin \text{SU}(1, 1)$. Then we could generally state that $S \in \text{SL}(2, \mathbb{C})$, meaning that the Möbius method should be adjusted to a more general representation, i.e.,

$$\mathbf{S} = \begin{pmatrix} S_{11} & S_{12} \\ S_{21} & S_{22} \end{pmatrix} \rightarrow w = \frac{S_{11}w_0 + S_{12}}{S_{21}w_0 + S_{22}},$$

with $S_{11}S_{22} - S_{12}S_{21} = 1$. This would in principle force the Riccati equation (14) to take its complete form, with an additional w term being included, and would result in the appearance of constants, depended on the two coupling coefficients of the modulated waveguides, multiplying each term. Then the variable ψ will effectively become complex $\psi \in \mathbb{C}$ so that $w = x \exp(iy)$, with $x, y \in \mathbb{R}$, meaning that information will then be encoded in two variables. Such a generalization is also required to include optical absorption but is beyond the scope of the present work.

IV. UNIFORM BRAGG GRATINGS

A. Adler equation

It turns out that Eq. (15) has an analytic solution in a closed form for the case of linear detuning, where $\varphi = \delta kz$, with $\delta k = 2\bar{n}k_0 - K_0$ the z -independent detuning parameter.

$$\psi(z, \lambda) = 2 \tan^{-1} \left(\frac{\frac{\delta k}{2\Delta} \cos\left(\frac{\psi_0 - \varphi}{2}\right) \sinh(\Delta z) + \sin\left(\frac{\psi_0 - \varphi}{2}\right) \cosh(\Delta z) + \frac{\kappa}{\Delta} \cos\left(\frac{\psi_0 + \varphi}{2}\right) \sinh(\Delta z)}{-\frac{\delta k}{2\Delta} \sin\left(\frac{\psi_0 - \varphi}{2}\right) \sinh(\Delta z) + \cos\left(\frac{\psi_0 - \varphi}{2}\right) \cosh(\Delta z) + \frac{\kappa}{\Delta} \sin\left(\frac{\psi_0 + \varphi}{2}\right) \sinh(\Delta z)} \right), \quad (18)$$

where $\Delta = [\kappa^2 - (\delta k/2)^2]^{1/2}$ is an eigenvalue of the characteristic matrix of Eq. (5). At $\delta k = \pm 2\kappa$, we can simply take $\lim_{\delta k \rightarrow \pm 2\kappa} \psi$ and simplify Eq. (18).

Identifying the parameters P and Q from Eq. (18) is not readily accessible but it is feasible since we established that Eq. (17) has Möbius-like solutions. Indeed, by expressing

$$w = \frac{1 + ui}{1 - ui} \quad \text{and} \quad w_0 = \frac{1 + u_0 i}{1 - u_0 i},$$

where $u = \tan(\psi/2)$ and $u_0 = \tan(\psi_0/2)$, and after some algebraic manipulations, we eventually get w to the form of Eq. (13) and identify the same parameters as those seen in Eqs. (4) and (5) in [18], specifically

$$P(z) = e^{-i\delta kz/2} p(z) \quad \text{and} \quad Q(z) = e^{-i\delta kz/2} q(z), \quad (19)$$

where

$$p(z) = \cosh(\Delta z) + i \frac{\delta k}{2\Delta} \sinh(\Delta z),$$

$$q(z) = i \frac{\kappa}{\Delta} \sinh(\Delta z).$$

Changing the variable according to $f = \psi + \delta kz$, Eq. (15) reduces to

$$\frac{df}{dz} = 2\kappa \cos f + \delta k, \quad (17)$$

which is the so-called Adler equation [48], typically giving an oscillator's phase as a function of time. Equations of this type describe Josephson junctions [49] and were recently studied in the context of laser physics for injection locking [50]. Comparing Eq. (17) with Eq. (21) in [51], it is straightforward to realize that they are identical, provided $A = 2\kappa$, $\lambda_{\text{Adl}} = \delta k/2\kappa$, and $\beta = \pi/2$. This is no surprise since a variety of coupled oscillators, with obvious similarity to CWEs, are known to be expressed via the Adler equation, the solutions of which are proved in Appendix D in [51] to be Möbius maps. Such a connection is particularly intriguing and N -dimensional optical systems modeled by globally coupled equations of the type

$$\frac{dA_j}{dz} = X(A_1, \dots, A_N) + \Psi(A_1, \dots, A_N) \cos A_j,$$

with $j = 1, \dots, N$ and X and Ψ independent of the subscript j being 2π periodic in each argument, would be of great interest to examine in the context of optics.

With boundary data $z \rightarrow z_0$ and $f_0 \rightarrow \psi_0 + \delta kz_0$, Eq. (17) can be integrated as

$$\int_{f_0}^f \frac{df}{1 + (2\kappa/\delta k) \cos f} = \delta k(z - z_0),$$

where the integral is calculated via the Weierstrass substitutions $t = \tan(f/2)$ and $t_0 = \tan(f_0/2)$. After some algebraic manipulations, the solution to Eq. (15) is found to be

Thus, we have demonstrated the fundamental reason of why our proposed method yields the well-known analytic result for uniform Bragg gratings seen, e.g., in [52].

At this point, we note that the transfer matrix

$$\tilde{\mathbf{S}} = \begin{pmatrix} p & q \\ q^* & p^* \end{pmatrix} \quad (20)$$

solves Eq. (5) and may be naturally related to a Möbius transformation $w_{\tilde{s}} = e^{iK_0 z} w$, where w is that of Eq. (13). We also note that it is trivial to reconstruct the transfer matrix for the actual electric fields. In fact, for $E = A^+ \exp(i\bar{k}z) + A^- \exp(-i\bar{k}z)$, where $\bar{k} = \bar{n}k_0$, it reads

$$\mathbf{S}_E = \begin{pmatrix} e^{iK_0 z/2} p & e^{iK_0 z/2} q \\ e^{-iK_0 z/2} q^* & e^{-iK_0 z/2} p^* \end{pmatrix}. \quad (21)$$

The intensity reflectance and transmittance of a uniform Bragg grating of length L are obtained by imposing the

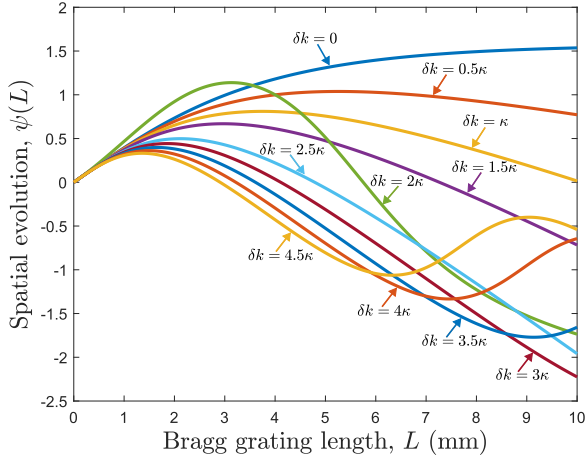


FIG. 1. Spatial evolution of ψ as a function of the Bragg grating length L for various detuning parameters δk , as per Eq. (18). The base parameters are $\Lambda = 0.538\,194\ \mu\text{m}$, $\bar{n} = 1.44$, $\delta\bar{n} = 10^{-4}$, and $\psi_0 = 0$.

boundary condition $A^-(L) = 0$. These are, respectively,

$$R = |r|^2 = \left| \frac{A^-(0)}{A^+(0)} \right|^2 = \left| \frac{-Q^*(L)}{P^*(L)} \right|^2 \quad \text{and}$$

$$T = |t|^2 = \left| \frac{A^+(L)}{A^+(0)} \right|^2 = \left| \frac{1}{P^*(L)} \right|^2.$$

In Fig. 1 the spatial evolution of ψ with the grating length is shown for various detuning parameters δk . By contrast, Fig. 2 depicts the spectral evolution of ψ for fixed grating length and scanning wavelength. Both figures refer to linear detuning.

B. The photonic band gap revisited

The condition $\Delta \in \mathbb{R}$ defines the Bragg zone and in the absence of loss or gain, Fig. 1 indicates that curves lying inside the Bragg zone have no inflection points whereas outside, where $\Delta = |\Delta| i \in \mathbb{C}$, they have at least one. This simple

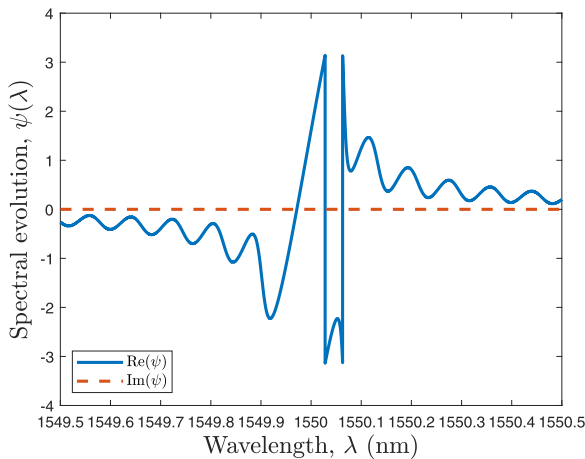


FIG. 2. Spectral evolution of ψ as a function of the wavelength λ for fixed Bragg grating length $L = 10\ \text{mm}$, as per Eq. (18). The parameters are the same as those of Fig. 1.

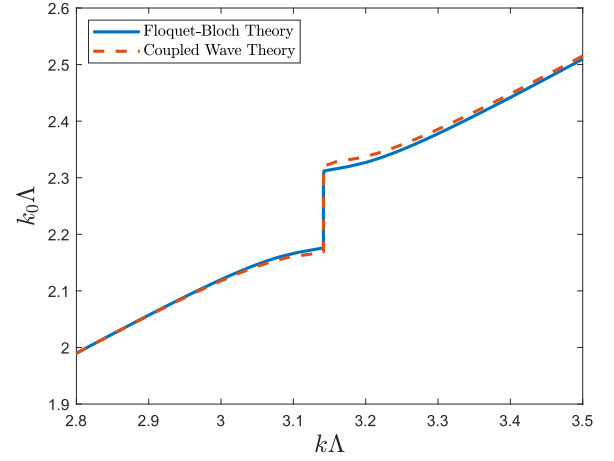


FIG. 3. Dispersion relation of uniform Bragg gratings for one harmonic, accessed via Floquet-Bloch theory and CWT [as per Eq. (22)]. The parameters are $\Lambda = 0.464\,29\ \mu\text{m}$, $\bar{n} = 1.4$, and $\delta\bar{n} = 0.1$. Material or waveguide dispersion is neglected.

criterion is easily verified by exploring the sign of $d^2\psi/dz^2$ and it is consistent with the stability condition $|\lambda_{\text{Adl}}| \leq 1$ of the Adler equation in [51].

The general dispersion relation of uniform Bragg gratings can be accessed by expanding the components of the forward propagating field, as identified in Eq. (21). From the various exponential terms, we see that the possible wave numbers k supported by the medium must satisfy

$$k = \frac{K_0}{2} + \text{sgn}(\delta k) \left[\left(\bar{n}k_0 - \frac{K_0}{2} \right)^2 - \left(\frac{k_0\delta\bar{n}}{2} \right)^2 \right]^{1/2}, \quad (22)$$

where $\text{sgn}(\delta k)$ ensures that $k \rightarrow 0$ as $k_0 \rightarrow 0$ and that $k \rightarrow \bar{n}k_0$ as $k_0 \rightarrow \infty$. Observing Eq. (22), it is evident that a photonic band gap, similar to that of photonic crystals, exists at

$$k_0 \approx \frac{K}{2\bar{n}} \left(1 \pm \frac{\delta\bar{n}}{2\bar{n}} \right).$$

In this regime, the wave vector k has a constant real part and a nonzero imaginary, indicating strong attenuation, and wave propagation is not allowed. This is visualized in Fig. 3, where the dispersion obtained via CWT for one harmonic is found in excellent agreement with that of the exact Floquet-Bloch theory, where a stepwise refractive index variation is assumed [53]. The dispersion expression of Eq. (22) is equivalent to the phase rotation number η of Eq. (11) in [51] if $\lambda_{\text{eig}} = -e^\eta$, where λ_{eig} is an eigenvalue of the matrix in Eq. (20), as discussed in [33].

The abovementioned classic approaches can be consistently related to the Möbius transformation method. As far as dispersion is concerned, it is actually the electric fields that we are ultimately interested in. Furthermore, the grating dispersion characteristics must be independent of its length, assuming no material or waveguide dispersion. Therefore, we consider a unit-cell grating of length equal to the period Λ of the refractive index sinusoidal modulation and realize that the electric-field transfer matrix of Eq. (21) reduces to $\hat{\mathbf{S}}(\Lambda)$, where we have dropped the -1 factor for simplicity. The

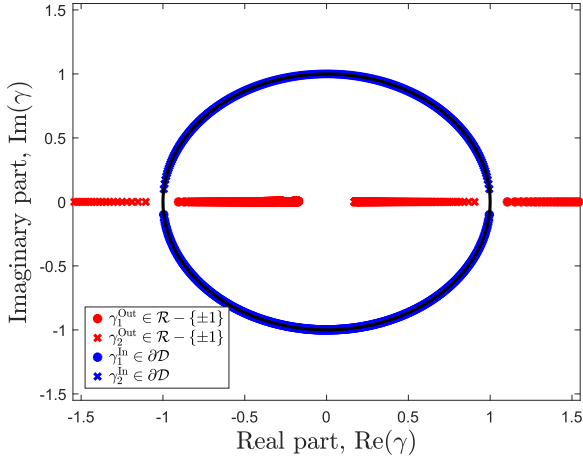


FIG. 4. Fixed points γ of the Möbius transformation $w_{\tilde{S}(\Lambda)}$ in the complex plain for various detuning parameters in the range $\delta k \in [-6\kappa, 6\kappa]$. The Bragg grating length is set to Λ and the parameters are the same as those of Fig. 3.

eigenvalues of $\tilde{S}(\Lambda)$ are found to be

$$\lambda_{\text{eig}} = \text{Re}[p(\Lambda)] \pm (\{\text{Re}[p(\Lambda)]\}^2 - 1)^{1/2}, \quad (23)$$

while the associated Möbius transformation's fixed points, found by solving $\gamma = w_{\tilde{S}(\Lambda)}(\gamma)$, are

$$\gamma = \frac{\pm(|q(\Lambda)|^2 - \{\text{Im}[p(\Lambda)]\}^2)^{1/2} + i \text{Im}[p(\Lambda)]}{q^*},$$

being related via $\lambda_{\text{eig}} = q^*(\Lambda)\gamma + p^*(\Lambda)$. The equivalent inside-the-Bragg-zone condition of Sec. III in [33] (or of Sec. 3 in [54]), for $\text{SU}(1, 1)$ symmetric structures, $|\text{Re}[p(\Lambda)]| \geq 1$, leads to real eigenvalues and $|\gamma| = 1$. It follows that the fixed points of $w_{\tilde{S}(\Lambda)}$ lie on the unit circle ∂D for wavelengths inside the Bragg zone and either inside or outside ∂D otherwise. For linear detuning, the latter are fixed on the real axis $\mathbb{R} - \{\pm 1\}$, as illustrated in Fig. 4. Tracing back to the corresponding wavelength of each fixed point on ∂D estimates the band gap. We are thus led to the following definition of a photonic band gap: *The photonic band gap of a periodic dielectric structure consists of the fixed points of $w_{\tilde{S}}$ laying on the unit circle.* Importantly, this alternative definition is not restricted to linear detuning, being applicable to any $\text{SU}(1, 1)$ symmetrical structure with arbitrarily complex refractive index modulation. In fact, Eq. (23) implies that

$$\lambda_{\text{eig}}^{(1)} + \lambda_{\text{eig}}^{(2)} = -2 \text{Re}[p(\Lambda)] \quad \text{and} \quad \lambda_{\text{eig}}^{(1)} \lambda_{\text{eig}}^{(2)} = 1.$$

Then there are two possibilities: Either $\lambda_{\text{eig}}^{(1)} \lambda_{\text{eig}}^{(2)} \in \mathbb{C}$ or $\lambda_{\text{eig}}^{(1)} \lambda_{\text{eig}}^{(2)} \in \mathbb{R}$. In the latter, following the arguments of [33], we may write $\lambda_{\text{eig}}^{(1)} = \pm e^\eta$ and $\lambda_{\text{eig}}^{(2)} = \pm e^{-\eta}$, which clearly demonstrates the nonoscillating field behavior, a signature of the photonic band gap. With the eigenvalues being purely real, it is straightforward to show that

$$|\gamma|^2 = \frac{|\lambda_{\text{eig}}^{(1,2)} - p^*|^2}{|p|^2 - 1} = 1 \Rightarrow |\gamma| = 1.$$

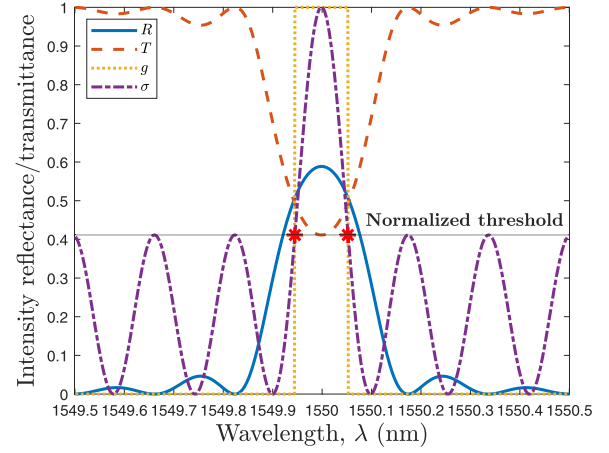


FIG. 5. Classification of the Möbius transformation and the Bragg zone as per Eq. (24), alongside the optical spectrum. The Bragg grating length is $L = 5$ mm and the parameters are the same as those of Fig. 1. At the starred points, g and σ coincide.

Hence, the introduced definition of the photonic band gap is also applicable to cases of arbitrarily complex refractive index modulation scenarios as we have made no assumptions about p .

A further interesting aspect of the photonic band gap is related to the general classification of the Möbius transformation, following an idea proposed in [55,56]. In uniform loss- and gain-free gratings, the trace of the matrix in Eq. (20) turns out to be real and classifies the transformation. For $\sigma = [\text{tr}(\tilde{S})]^2$, the transformations may be elliptic ($0 \leq \sigma < 4$), parabolic ($\sigma = 4$), or hyperbolic ($4 < \sigma < \infty$), although there exist other classification classes too. This is expected since the trace of transfer matrices is known to be related to the so-called Bloch angle via $\text{tr}(\tilde{S}) = 2 \cos \theta_B$ [see Eq. (1.55) in [57]], where $\lambda_{\text{eig}} = e^{\pm i\theta_B}$ (cf. phase rotation number η). Outside the Bragg zone, the Möbius representation is elliptic, at the edges it crosses the $\sigma_{\text{th}} = 4$ threshold to become parabolic, and inside is hyperbolic. These are visualized in Fig. 5 where the optical spectrum of a uniform Bragg grating is plotted alongside the normalized to their peak values σ , σ_{th} , and a piecewise rectangular function identifying the Bragg zone via Δ as

$$g(\lambda) = \begin{cases} 1 & \text{if } \text{Im}[\Delta(\lambda)] = 0 \\ 0 & \text{if } \text{Im}[\Delta(\lambda)] \neq 0 \end{cases}. \quad (24)$$

At the threshold crossing points, σ and g coincide, thus revealing yet another aspect of the Bragg zone: At the two edges marking the parabolic regime, the transformation's fixed points concur taking the values $\gamma_1 = \gamma_2 = \pm 1$ missing from the real axis of Fig. 4. This substantiates the fact that parabolic Möbius transformations have only one fixed point. Such geometrical approaches to classic problems in optics have recently attracted much attention (see, e.g., [58]) and appear to serve as convenient platforms for exploring fundamentally complicated concepts.

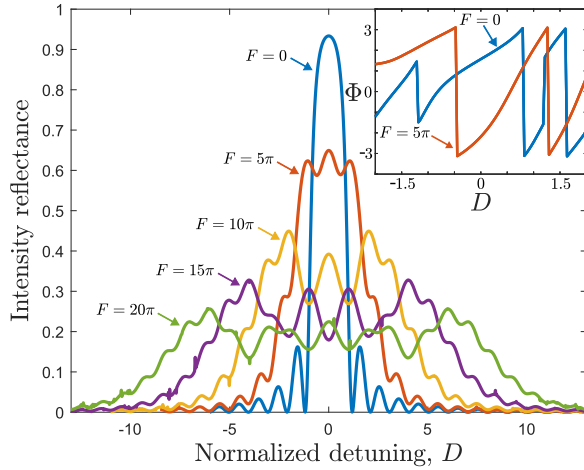


FIG. 6. Linearly chirped Bragg grating intensity reflectance for various chirp coefficients F . The Bragg grating length is $L = 10$ mm and the parameters are the same as those of Fig. 1. The inset illustrates the phase Φ of the reflection coefficient $r = |r|e^{i\Phi}$ for $F = 0$ and $F = 5\pi$.

V. ADVANCED REFRACTIVE INDEX MODULATION SCENARIOS

A. Linear and quadratic chirping

In the linear chirping case, the refractive index variation along the grating length is modeled via $\Delta k(z) = (2F/L^2)z$, where the constant F is the chirp coefficient measuring the degree of chirping [5,12]. At this instance, Eq. (2) acquires an additional z^2 term to become

$$\varphi = [2\bar{n}k_0 - K_0 - (F/L^2)z]z.$$

By defining an effective z -dependent detuning as $\delta k_{\text{eff}}(z) = 2\bar{n}k_0 - K_0 - (F/L^2)z$, it is evident that linear chirping changes the Bragg wavelength along z , thus broadening and shifting the spectrum with the direction of the shift, towards the red or the blue, depending on the sign of F . Then the expression for the phase term can be substituted into Eq. (15), which is now written as

$$\frac{d\psi}{dz} = 2\kappa \cos[\psi + \delta k_{\text{eff}}(z)z]. \quad (25)$$

Unlike the previous case, Eq. (25) cannot be analytically integrated and the algorithm of Sec. III C must be implemented. We note that in the Appendix in [59], an analytic solution to the CWEs for linear chirping is reported, without however solving Eq. (25). Their proposed solution involves the highly complex Whittaker function and the authors underline the difficulty in assessing its validity for nonlinear chirping. We are confident that our Eq. (25) will lead to analytic solutions for nontrivial cases and employing group theory appears as a favorable candidate.

In Fig. 6 the intensity reflectance of a linearly chirped Bragg grating is plotted against the normalized detuning $D = \delta k_{\text{eff}}(L)L/2\pi$ for large values of F . An increment of F broadens the spectrum, decreasing simultaneously its peak value. The same algorithm can be applied for any kind of grating pitch variation. In the case of quadratic chirping, where $\Delta K(z) = (12F/L^3)z^2$, the intensity reflectance is illustrated in

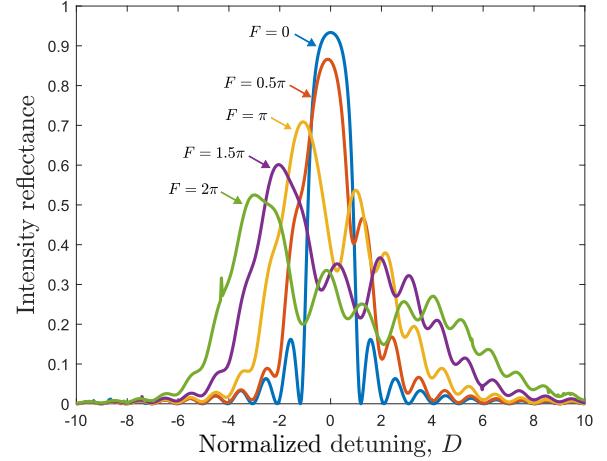


FIG. 7. Quadratically chirped Bragg grating intensity reflectance for various chirp coefficients F . The Bragg grating length is $L = 10$ mm and the parameters are the same as those of Fig. 1.

Fig. 7. The symmetrical response of the linearly chirped Bragg grating is compared to the asymmetrical of the quadratically chirped, whereby an increment of the chirp coefficient causes the reduction of the side lobes' peaks on the right of the Bragg wavelength and their level's accretion on the left (see [5]).

B. Apodized Bragg gratings

Up until this point, the grating coupling coefficient has been assumed to be z -independent. As it is a common practice to write fiber Bragg gratings via laser beams with a Gaussian profile [12], the beam's characteristics will be inherited by the refractive index modulation profile. Then the coupling coefficient will become z -dependent and may be modeled similarly to Eq. (10) in [7] as

$$\kappa(z) = \frac{\pi \delta \bar{n}}{\lambda_0} \exp \left[-16 \frac{(z - L/2)^2}{L^2} \right] \quad (26)$$

so that it gradually decreases at the ends of the coupling region, thus suppressing the side lobes. As long as Eq. (26) remains real, the Hermiticity of the characteristic matrix \mathbf{M} is uninterrupted and the method of Sec. III is applicable. As depicted in Fig. 8, using a Gaussian taper function, the optical response becomes smoother and the side lobes are suppressed. An increment of the grating length will asymptotically provide an almost-top-flat response for a sufficiently broad bandwidth. Moreover, considering the insets of Figs. 6 and 8 for, say, $F = 0$, yet another advantage of apodization is revealed: The phase response becomes approximately linear, which is much desired for dispersion compensation (see [60]).

Comparing Figs. 6 and 8, the Gaussian taper function of Eq. (26) may have suppressed the side lobes but has also decreased the peak values of the intensity reflectances. A compromise could be achieved by using a raised-cosine profile for the coupling coefficient,

$$\kappa(z) = \frac{\pi \delta \bar{n}}{\lambda_0} \frac{1}{2} \left[1 + \cos \left(\frac{\pi(z - L/2)}{L} \right) \right]. \quad (27)$$

The resulting optical spectrum can be seen in Fig. 9.

Different apodization profiles can be combined with any kind of chirping for tailor-made applications. Our proposed

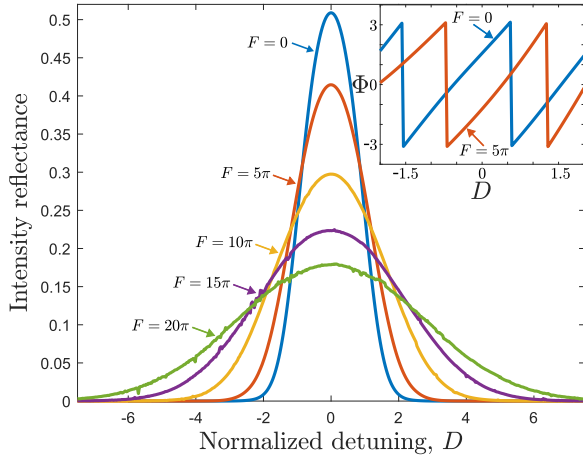


FIG. 8. Gaussian apodized linearly chirped Bragg grating intensity reflectance. The scenario is that of Fig. 6 and the coupling coefficient profile is given by Eq. (26). The inset illustrates the phase Φ of the reflection coefficient $r = |r|e^{i\Phi}$ for $F = 0$ and $F = 5\pi$.

method can easily access every possible scenario, with potential applications in phase-reconstruction problems where for a targeted optical spectrum (peak reflectance, bandwidth, and time delay) one may have to determine the grating parameters by trial-and-error. In such problems, an analytic solution is in principle unachievable, particularly for strong gratings. This topic is part of the wider family of inverse scattering problems and optimization algorithms still attract scientific interest. The methods proposed in [61,62], which utilized the Hilbert transformation and were strictly based on causality and stability conditions that relate the amplitude of the response function to its phase, were found in [63] to significantly fail for realistic imperfect gratings. Currently, the two dominant synthesis techniques are the so-called genetic programming [64,65] and layer peeling [66,67] algorithms. In the first, a certain weighting mechanism is required and relies on a trial-and-error method for error estimation, with the main drawbacks being high complexity and long running times. In contrast, the

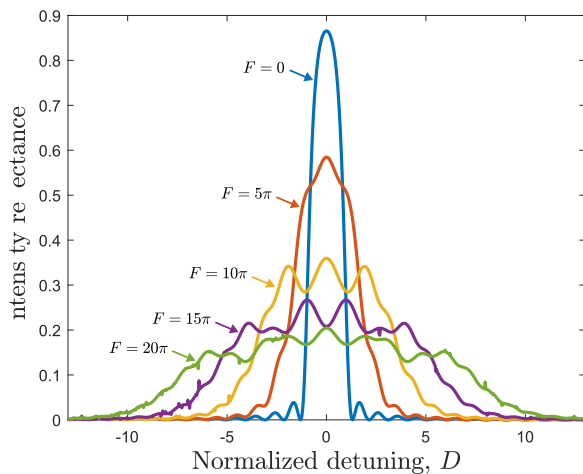


FIG. 9. Raised cosine apodized linearly chirped Bragg grating intensity reflectance. The scenario is that of Fig. 6 and the coupling coefficient profile is given by Eq. (27).

layer peeling algorithm (continuous or discrete) is based on evaluating the grating strength as waves propagate. Although it is by far the best technique proposed to date, in cases of strong gratings the algorithm is severely affected by noise. To deal with this, a regularization method was proposed in [68] which reduces the grating strength by a factor of μ with the price being a slight decrease in accuracy. The optimal value of μ can be found by trial-and-error algorithms and we contend that our method, which encodes all spectral information to a single real variable, might prove useful.

C. Cascaded Bragg gratings with slightly dissimilar pitches

In [18] the problem of two cascaded Bragg gratings of equal lengths $L/2$ and slightly dissimilar pitches $\Lambda_1 \neq \Lambda_2$ was addressed via the piecewise transfer-matrix approach. When cascading N gratings, there are three common pitfalls to be avoided. First, the transfer matrix strongly depends on the location l_0 where the amplitudes of the electric fields are presumed to be known. This implies that for $\mathbf{A}(l_0)$ known, the expression of Eq. (21) for $z = z - l_0$ does not lead to the correct spectrum and the formalism of Eq. (3) in [18] should be adopted instead. Second, if the transformation leading to Eq. (5) is preferred, as, e.g., in [9,10,12], the overall transfer matrix is not just

$$\tilde{\mathbf{S}} = \tilde{\mathbf{S}}_N(z_{N-1}, z_N) \cdots \tilde{\mathbf{S}}_1(z_0, z_1),$$

but the intermediate terms

$$\mathbf{N}_{j,j+1}(z_j) = \mathbf{M}_{j+1}(z_j) \cdot \mathbf{M}_j^{-1}(z_j),$$

where $j = 1, \dots, N - 1$ and

$$\mathbf{M}_j = \begin{pmatrix} e^{i\varphi_j/2} & 0 \\ 0 & e^{-i\varphi_j/2} \end{pmatrix}, \quad (28)$$

sandwiched between $\tilde{\mathbf{S}}_{j+1}(z_{j+1} - z_j)$ and $\tilde{\mathbf{S}}_j(z_j - z_{j-1})$ must be considered. Otherwise, no spectral hole will appear if the relevant condition $1/\Lambda_2 - 1/\Lambda_1 = 1/L$ of Eq. (20) in [18] is met. It is notable that the widely used CWEs description of Eq. (5) fails to capture the induced spectral hole, given its importance in sensing applications (see, e.g., [69,70]). Finally, gratings delineated by a phase discontinuity should not be modeled by phase matrices, similar to that of Eq. (28), but by the phase term of Eq. (2). In other respects, it will result in erroneous spectra, evident via simple phase-sensitive experiments (cf. Fig. 9 in [18]).

To demonstrate the success of our method in hiding such complexity, we compare the optical spectra of two cascaded gratings of slightly dissimilar pitches accessed via the revised transfer-matrix approach of [18] and via the Möbius transformation method. The compound grating has an overall transfer matrix

$$\mathbf{S}_{\text{total}} = \mathbf{S}_2 \cdot \mathbf{S}_1,$$

with elements given by

$$S_{11} = P_2(L/2)P_1(L/2) + Q_2(L/2)Q_1^*(L/2),$$

$$S_{12} = P_2(L/2)Q_1(L/2) + Q_2(L/2)P_1^*(L/2),$$

where P_i and Q_i ($i = 1, 2$) refer to a uniform grating segment of spatial period Λ_i and are calculated via the expressions (19). Also, $S_{21} = S_{12}^*$ and $S_{22} = S_{11}^*$.

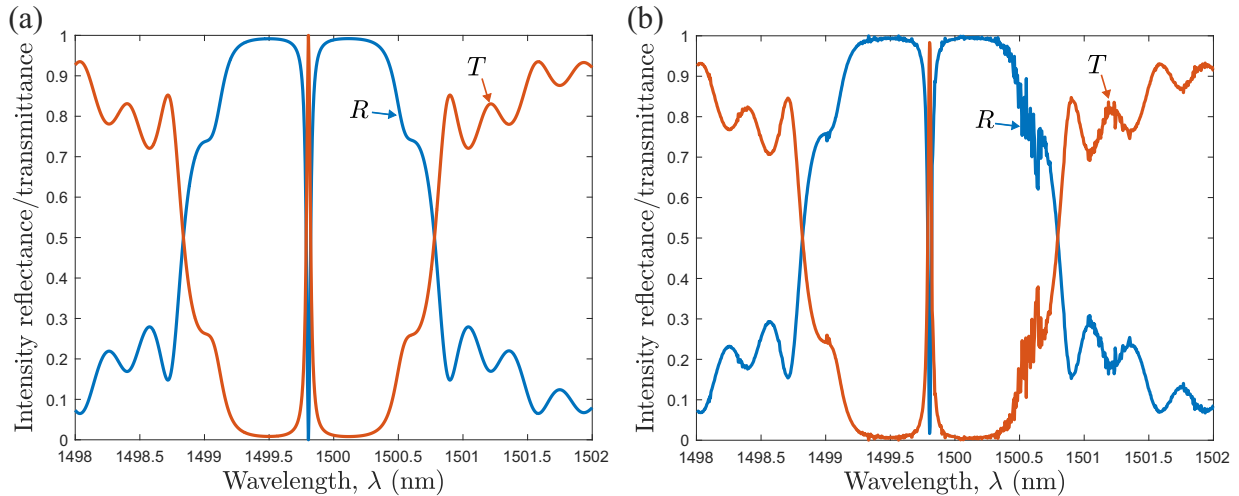


FIG. 10. Optical spectrum of two cascaded Bragg gratings of equal lengths $L/2$ and slightly dissimilar pitches $\Lambda_1 \neq \Lambda_2$ found via (a) the transfer matrix method and (b) the Möbius transformation method. The parameters are $\Lambda_1 = 0.51774 \mu\text{m}$, $\Lambda_2 = 0.51761 \mu\text{m}$, $n = 1.4486$, $L = 3 \times 10^{-3}/n$, and $\delta n = 10^{-3}$. The scanning wavelength resolution is set to 10^{-3} .

For the Möbius method, the only essential concern is the φ term of Eq. (15) which is now a discontinuous piecewise function, namely,

$$\varphi(z) = \begin{cases} \delta k_1 z, & 0 \leq z \leq L/2 \\ \delta k_2 z, & L/2 < z \leq L \end{cases}$$

for $\delta k_1 \neq \delta k_2$. The optical spectra of the two methods are compared in Fig. 10 for Λ_1 and Λ_2 such that they satisfy the spectral hole condition. Doubtlessly, both methods capture the induced spectral hole at $\lambda = \bar{n}(\Lambda_1 + \Lambda_2) = 1499.8 \text{ nm}$. The higher-order fluctuations are due to MATLAB's ODE solvers limitation when dealing with discontinuous functions which nevertheless clearly provide the necessary accuracy.

VI. CONCLUSIONS

Inspired by group theory, we applied a Möbius transformation to the CWEs of Bragg gratings which established a link between CWT and coupled oscillators and revealed insights into the photonic band gap of arbitrarily complex refractive index modulation scenarios. Restricting the action of

the transformation to the unit circle reduced the scalar CWEs to a first-order nonlinear differential equation of a single real variable. Exploring the geometrical properties of the transformation and numerically solving the equation led to algebraic identification of both the amplitude and phase of all elements of the transfer matrix. The method is fast, reliable, and in principle applicable to any phenomenon governed by CWEs with performance independent of the number of periods, being inherently continuous. Additionally, it may provide a useful tool for promptly reverse engineering Bragg gratings. We believe that our method can simplify the analysis and design of photonic structures governed by CWEs via an optics-based version of Smith charts. A next step will be a generalization to include optical absorption and modulated gain to examine structurally chiral media and \mathcal{PT} -symmetric Bragg gratings. Further applications in globally coupled oscillators appear within reach.

ACKNOWLEDGMENT

S. F. Koufidis wishes to acknowledge financial support from the Bodossaki Foundation.

-
- [1] R. Kashyap, *Fiber Bragg Gratings*, 2nd ed. (Academic Press, Burlington, MA, 2010).
- [2] K. O. Hill, B. Malo, F. Bilodeau, D. C. Johnson, and J. Albert, Bragg gratings fabricated in monomode photosensitive optical fiber by UV exposure through a phase mask, *Appl. Phys. Lett.* **62**, 1035 (1993).
- [3] G. E. Town, K. Sugden, J. A. R. Williams, I. Bennion, and S. B. Poole, Wide-band Fabry-Pérot-like filters in optical fiber, *IEEE Photon. Technol. Lett.* **7**, 78 (1995).
- [4] T. Feng, M. Wang, M. Jiang, X. Wang, F. Yan, Y. Suo, and X. Steve Yao, C-band 41-wavelength-switchable single-longitudinal-mode fiber laser with sub-kHz linewidth and high stability using a wide-band chirped Moiré fiber Bragg grating, *Laser Phys. Lett.* **16**, 025106 (2019).
- [5] H. Kogelnik, Filter response of nonuniform almost-periodic structures, *Bell Syst. Tech. J.* **55**, 109 (1976).
- [6] P. A. Morton, V. Mizrahi, T. Tanbun-Ek, R. A. Logan, P. J. Lemaire, H. M. Presby, T. Erdogan, S. L. Woodward, J. E. Sipe, M. R. Phillips, A. M. Sergent, and K. W. Wecht, Stable single mode hybrid laser with high power and narrow linewidth, *Appl. Phys. Lett.* **64**, 2634 (1994).
- [7] F. Ouellette, Dispersion cancellation using linearly chirped Bragg grating filters in optical waveguides, *Opt. Lett.* **12**, 847 (1987).
- [8] M. E. Fermann, K. Sugden, and I. Bennion, High-power soliton fiber laser based on pulse width control with chirped fiber Bragg gratings, *Opt. Lett.* **20**, 172 (1995).

- [9] R. Zengerle and O. Leminger, Phase-shifted Bragg-grating filters with improved transmission characteristics, *J. Lightw. Technol.* **13**, 2354 (1995).
- [10] G. P. Agrawal and S. Radic, Phase-shifted fiber Bragg gratings and their application for wavelength demultiplexing, *IEEE Photon. Technol. Lett.* **6**, 995 (1994).
- [11] F. Bakhti and P. Sansonetti, Design and realization of multiple quarter-wave phase-shifts UV-written bandpass filters in optical fibers, *J. Lightw. Technol.* **15**, 1433 (1997).
- [12] T. Erdogan, Fiber grating spectra, *J. Lightw. Technol.* **15**, 1277 (1997).
- [13] S. G. Johnson, M. L. Povinelli, P. Bienstman, M. Skorobogatiy, M. Soljacic, M. Ibanescu, E. Lidorikis, and J. D. Joannopoulos, *Proceedings of 2003 5th International Conference on Transparent Optical Networks, 2003* (IEEE, Piscataway, 2003), Vol. 1, pp. 103–109.
- [14] J. E. Sipe, L. Poladian, and C. Martijn de Sterke, Propagation through nonuniform grating structures, *J. Opt. Soc. Am. A* **11**, 1307 (1994).
- [15] H. V. Baghdasaryan and T. M. Knyazyan, Modelling of strongly nonlinear sinusoidal Bragg gratings by the method of single expression, *Opt. Quantum Electron.* **32**, 869 (2000).
- [16] M. Yamada and K. Sakuda, Analysis of almost-periodic distributed feedback slab waveguides via a fundamental matrix approach, *Appl. Opt.* **26**, 3474 (1987).
- [17] L. Wei and J. W. Y. Lit, Phase-shifted Bragg grating filters with symmetrical structures, *J. Lightw. Technol.* **15**, 1405 (1997).
- [18] M. W. McCall, On the application of coupled mode theory for modeling fiber Bragg gratings, *J. Lightw. Technol.* **18**, 236 (2000).
- [19] S. Watanabe and S. H. Strogatz, Constants of motion for superconducting Josephson arrays, *Physica D* **74**, 197 (1994).
- [20] C. J. Goebel, Comment on “Constants of motion for superconductor arrays”, *Physica D* **80**, 18 (1995).
- [21] D. A. Fish, A. K. Powell, and T. J. Hall, A steady state solution to four-wave mixing in the transmission geometry utilising the SU(2) group symmetry, *Opt. Commun.* **88**, 281 (1992).
- [22] A. K. Powell, D. A. Fish, and T. J. Hall, Solution to four-wave mixing in the reflection geometry utilising the SU(1,1) group symmetry, *Opt. Commun.* **89**, 68 (1992).
- [23] S. A. Marvel, R. E. Mirollo, and S. H. Strogatz, Identical phase oscillators with global sinusoidal coupling evolve by Möbius group action, *Chaos* **19**, 043104 (2009).
- [24] F. Abrishamian, S. Sato, and M. Imai, A new method of solving multimode coupled equations for analysis of uniform and non-uniform fiber Bragg gratings and its application to acoustically induced superstructure modulation, *Opt. Rev.* **12**, 467 (2005).
- [25] F. Abrishamian, Y. Nakai, S. Sato, and M. Imai, An efficient approach for calculating the reflection and transmission spectra of fiber Bragg gratings with acoustically induced microbending, *Opt. Fiber Technol.* **13**, 32 (2007).
- [26] F. Abrishamian, S. Sato, and M. Imai, Analysis of solving multimode-coupled equations and its improvement for modulated fiber Bragg gratings, *Appl. Opt.* **48**, 4031 (2009).
- [27] P. Hartman, *Ordinary Differential Equations*, 2nd ed. (SIAM, Philadelphia, 2002), Chap. IV.
- [28] G. Söderlind and L. Wang, Adaptive time-stepping and computational stability, *J. Comput. Appl. Math.* **185**, 225 (2006).
- [29] M. Prabhugoud and K. Peters, Modified transfer matrix formulation for Bragg grating strain sensors, *J. Lightw. Technol.* **22**, 2302 (2004).
- [30] M. Kulishov, J. M. Laniel, N. Bélanger, J. Azaña, and D. V. Plant, Nonreciprocal waveguide Bragg gratings, *Opt. Express* **13**, 3068 (2005).
- [31] A. Yariv, Coupled-mode theory for guided-wave optics, *IEEE J. Quantum Electron.* **9**, 919 (1973).
- [32] D. H. Sattinger and O. L. Weaver, *Lie Groups and Algebras with Applications to Physics, Geometry, and Mechanics* (Springer, Berlin, 1986), Chap. 1.
- [33] N. Matuschek, F. X. Kartner, and U. Keller, Exact coupled-mode theories for multilayer interference coatings with arbitrary strong index modulations, *IEEE J. Quantum Electron.* **33**, 295 (1997).
- [34] N. Byrnes and M. R. Foreman, Symmetry constraints for vector scattering and transfer matrices containing evanescent components: Energy conservation, reciprocity, and time reversal, *Phys. Rev. Res.* **3**, 013129 (2021).
- [35] J. D. Olson and J. L. Mace, Wave function confinement via transfer matrix methods, *J. Math. Phys.* **44**, 1596 (2003).
- [36] L. L. Sánchez-Soto, J. J. Monzón, A. G. Barriuso, and J. F. Cariñena, The transfer matrix: A geometrical perspective, *Phys. Rep.* **513**, 191 (2012).
- [37] A. G. Barriuso, J. J. Monzón, and L. L. Sánchez-Soto, General unit-disk representation for periodic multilayers, *Opt. Lett.* **28**, 1501 (2003).
- [38] L. V. Ahlfors, *Conformal Invariants: Topics in Geometric Function Theory* (McGraw-Hill, New York, 1973), Chap. 1.
- [39] P. H. Smith, *Electronic Applications of the Smith Chart: In Waveguide, Circuit, and Component Analysis*, 2nd ed. (SciTech, Chennai, 1995).
- [40] T. Needham, *Visual Complex Analysis* (Oxford University Press, Oxford, 1997).
- [41] A. Pikovsky and M. Rosenblum, Partially Integrable Dynamics of Hierarchical Populations of Coupled Oscillators, *Phys. Rev. Lett.* **101**, 264103 (2008).
- [42] A. Galda and V. M. Vinokur, Linear dynamics of classical spin as Möbius transformation, *Sci. Rep.* **7**, 1168 (2017).
- [43] J. W. Brown and R. V. Churchill, *Complex Variables and Applications*, 9th ed. (McGraw-Hill, New York, 2014), Chap. 10.
- [44] Y. Lipman and T. Funkhouser, Möbius voting for surface correspondence, *ACM Trans. Graph.* **28**, 1 (2009).
- [45] O. Omel'chenko, Periodic orbits in the Ott-Antonsen manifold, [arXiv:2206.01481](https://arxiv.org/abs/2206.01481).
- [46] Z. Lin, H. Ramezani, T. Eichelkraut, T. Kottos, H. Cao, and D. N. Christodoulides, Unidirectional Invisibility Induced by \mathcal{PT} -Symmetric Periodic Structures, *Phys. Rev. Lett.* **106**, 213901 (2011).
- [47] J. Čtyrký, V. Kuzmiak, and S. Eyderman, Waveguide structures with antisymmetric gain/loss profile, *Opt. Express* **18**, 21585 (2010).
- [48] R. Adler, A study of locking phenomena in oscillators, *Proc. IRE* **34**, 351 (1946).
- [49] K. Wiesenfeld, P. Colet, and S. H. Strogatz, Synchronization Transitions in a Disordered Josephson Series Array, *Phys. Rev. Lett.* **76**, 404 (1996).
- [50] L. Danner, C. Padurariu, J. Ankerhold, and B. Kubala, Injection locking and synchronization in Josephson photonics devices, *Phys. Rev. B* **104**, 054517 (2021).

- [51] C. C. Gong, R. Toenjens, and A. Pikovsky, Coupled Möbius maps as a tool to model Kuramoto phase synchronization, *Phys. Rev. E* **102**, 022206 (2020).
- [52] K. Okamoto, *Fundamentals of Optical Waveguides* (Elsevier, Amsterdam, 2021).
- [53] C. Elachi, Waves in active and passive periodic structures: A review, *Proc. IEEE* **64**, 1666 (1976).
- [54] U. Bandelow and U. Leonhardt, Light propagation in one-dimensional lossless dielectrics: Transfer matrix method and coupled mode theory, *Opt. Commun.* **101**, 92 (1993).
- [55] L. L. Sánchez-Soto, J. J. Monzón, T. Yonte, and J. F. Cariñena, Simple trace criterion for classification of multilayers, *Opt. Lett.* **26**, 1400 (2001).
- [56] J. J. Monzón, A. G. Barriuso, L. L. Sánchez-Soto, and J. M. Montesinos-Amilibia, Geometrical interpretation of optical absorption, *Phys. Rev. A* **84**, 023830 (2011).
- [57] E. Akkermans, G. V. Dunne, and E. Levy, Wave propagation in one dimension: Methods and applications to complex and fractal structures, in *Optics of Aperiodic Structures*, edited by L. D. Negro (Stanford, Singapore, 2013), Chap. 10.
- [58] J. J. Monzón, A. G. Barriuso, J. M. Montesinos-Amilibia, and L. L. Sánchez-Soto, Geometrical aspects of \mathcal{PT} -invariant transfer matrices, *Phys. Rev. A* **87**, 012111 (2013).
- [59] M. Matsuhara, K. O. Hill, and A. Watanabe, Optical-waveguide filters: Synthesis, *J. Opt. Soc. Am.* **65**, 804 (1975).
- [60] K. O. Hill, S. Thériault, B. Malo, F. Bilodeau, T. Kitagawa, D. C. Johnson, J. Albert, K. Takiguchi, T. Kataoka, and K. Hagimoto, Chirped in-fibre Bragg grating dispersion compensators: Linearization of dispersion characteristic and demonstration of dispersion compensation in 100 km, 10 Gbit/s optical fibre link, *Electron. Lett.* **30**, 1755 (1994).
- [61] M. A. Muriel and A. Carballar, Phase reconstruction from reflectivity in uniform fiber Bragg gratings, *Opt. Lett.* **22**, 93 (1997).
- [62] A. Carballar and M. A. Muriel, Phase reconstruction from reflectivity in fiber Bragg gratings, *J. Lightw. Technol.* **15**, 1314 (1997).
- [63] J. Skaar and H. E. Engan, Phase reconstruction from reflectivity in fiber Bragg gratings, *Opt. Lett.* **24**, 136 (1999).
- [64] J. Skaar and K. M. Risvik, A genetic algorithm for the inverse problem in synthesis of fiber gratings, *J. Lightw. Technol.* **16**, 1928 (1998).
- [65] S. Zheng, N. Zhang, Y. Xia, and H. Wang, Research on non-uniform strain profile reconstruction along fiber Bragg grating via genetic programming algorithm and interrelated experimental verification, *Opt. Commun.* **315**, 338 (2014).
- [66] J. Skaar, L. Wang, and T. Erdogan, On the synthesis of fiber Bragg gratings by layer peeling, *IEEE J. Quantum Electron.* **37**, 165 (2001).
- [67] G. A. Cranch and G. M. H. Flockhart, Tools for synthesising and characterising Bragg grating structures in optical fibres and waveguides, *J. Mod. Opt.* **59**, 493 (2012).
- [68] J. Skaar and R. Feced, Reconstruction of gratings from noisy reflection data, *J. Opt. Soc. Am. A* **19**, 2229 (2002).
- [69] L. Michaille, M. W. McCall, Y. C. Lai, and J. A. R. Williams, Analysis of single and multiple, non-permanent, tunable, birefringent spectral holes in a fibre-Bragg grating stop-band produced via uniaxial pressure, *Opt. Commun.* **222**, 1 (2003).
- [70] R. Correia, E. Chehura, S. W. James, and R. P. Tatam, A pressure sensor based upon the transverse loading of a sub-section of an optical fibre Bragg grating, *Meas. Sci. Technol.* **18**, 3103 (2007).